Magnetic reconnection at the dayside magnetopause in global Lyon-Fedder-Mobarry simulations

J. E. Ouellette,[1] B. N. Rogers,[1] M. Wiltberger,[2] and J. G. Lyon[1]

Received 10 September 2009; revised 3 March 2010; accepted 23 March 2010; published 21 August 2010.

[1] We present a survey of magnetic reconnection at the dayside magnetopause using the Lyon-Fedder-Mobarry global magnetospheric simulation code. We explore simulations of the magnetospheric response under solar wind conditions with interplanetary magnetic field (IMF) clock angles of 0, 45, 90, 135, and 180 degrees. Defining the dayside reconnection rate as the total amount of magnetic flux per unit time that changes magnetic topology, we find the reconnection rate increases linearly from 45 to 135 degrees with more modest increases from 0 to 45 degrees and 135 to 180 degrees. Similar results are obtained using two other related definitions of the reconnection rate. We show the increase in the reconnection rate with greater IMF clock angles follows a trend in the orientation of the separator line relative to the solar wind magnetic field, a quantity that scales approximately as $\sin(\theta_{IMF}/2)$, as noted by Kan and Lee (1979). For northward IMF conditions, we apply a similar argument based on the width of weak $|\mathbf{B}|$ regions at the magnetopause. We find the simulations exhibit two qualitatively different reconnection processes. The first process we identify as three-dimensional topology merging along a separator line, in which solar wind and dipolar field lines reconnect, creating field lines with one foot point on the Earth and the other in the solar wind. For IMF angles of 45 and 90 degrees this topology merging is a predominantly antiparallel reconnection process concentrated near nulls in the magnetic cusps, while for larger IMF clock angles of 135 or 180 degrees the reconnection extends across belt-like regions spanning the subsolar point. For clock angles of 45 and 90 degrees we also identify a second type of reconnection process that is a three-dimensional form of guide field reconnection and typically occurs in regions along the separator line closer to the subsolar point. This process can mediate the reconnection of solar wind field lines with each other or can couple to the topology merging, leading to a subset of field lines that exhibit reconnection in multiple locations at the same moment of time.

Citation: Ouellette, J. E., B. N. Rogers, M. Wiltberger, and J. G. Lyon (2010), Magnetic reconnection at the dayside magnetopause in global Lyon-Fedder-Mobarry simulations, *J. Geophys. Res.*, *115*, A08222, doi:10.1029/2009JA014886.

1. Introduction

[2] Magnetic reconnection at the dayside magnetopause is widely believed to play an important role in the transport of magnetic flux and plasma into the Earth's magnetosphere. The three-dimensional complexity of the magnetopause geometry, however, has lead to enduring uncertainty about more specific questions, such as where the reconnection takes place, in what physical form it occurs, and even how reconnection should be defined. Concerning the latter question, in the magnetosphere there are four topologies of magnetic field lines [see, e.g., *Lau and Finn*, 1990]: solar wind or IMF field lines which extend out beyond the domain of interest at both ends, closed dipolar field lines that are connected to the Earth at both ends, and two classes of open field lines that touch the Earth's surface at either the northern or southern polar cap and extend into space at the other end. The surfaces that form the boundaries between volumes of different magnetic field topology are called separatrix surfaces, and the singular magnetic field line along which these surfaces intersect is called the separator line. By definition all four topologies of the magnetic field, solar wind, closed, and the two open topologies, converge on this line. As a result, the separator line, which typically cuts across the subsolar point on the magnetopause surface and connects magnetic null points on the dawn and dusk flanks, is the nexus of the dayside topology merging process. Probably the least ambiguous but most restrictive definition of magnetic reconnection in three-dimensional systems [e.g., *Greene*, 1993; *Boozer*, 1975] is based on the temporal growth of magnetic flux within a given topological category, a definition that unfortunately typically excludes

[1]Department of Physics and Astronomy, Dartmouth College, Hanover, New Hampshire, USA.
[2]High Altitude Observatory, National Center for Atmospheric Research, Boulder, Colorado, USA.

0148-0227/10/2009JA014886

the main case of interest here, namely, reconnection in a quasi-steady state magnetic geometry such as the magnetopause. At the other extreme [e.g., *Axford*, 1984; *Schindler et al.*, 1988; *Hesse and Schindler*, 1984], a less restrictive definition that applies to reconnection in all systems, time steady or not, is based on the breakdown of the frozen-in condition; magnetic reconnection is said to occur when two plasma elements that were connected by a magnetic field line at one time are no longer connected at some later time. Arguments have also been made for a broader definition based, for example, on the flow of plasma across separatrix surfaces [*Vasyliunas*, 1975]. Here, using a mixture of the latter two methods, we analyze the reconnection of IMF and dipolar field lines in global LFM simulations by tracking solar wind plasma fluid elements and frozen-in magnetic field lines as they approach the Earth, searching for a transition from a solar wind topology to a topology with one foot point on the Earth and the other in space. Defining the dayside reconnection rate as the total amount of magnetic flux per unit time that undergoes this topology transition, we find the reconnection rate increases linearly from 45 to 135 degrees with more modest increases from 0 to 45 degrees and from 135 to 180 degrees. The difference between the maximum rate (at due southward IMF) and minimum rate (due northward) is about a factor of 5 or 6. Similar results are also obtained using two other closely related definitions of the reconnection rate, one based on integrating the parallel electric field along the separator line and another based on a cross-polar-cap potential difference [e.g., *Siscoe et al.*, 2001].

[3] In addition to the total reconnection rate, the tracking of field lines in the simulations in many cases allows us to identify where and how topology merging actually takes place. For the majority of flux making the topology transition at any given moment in the simulation, the decoupling of the plasma and magnetic field motions can be clearly traced to a single spatially localized region on any given field line where the frozen-in condition is strongly violated. For IMF clock angles of 180 or 135 degrees, the reconnection is found to extend across broad, belt-like regions along the separator line, where the magnetopause and magnetosheath magnetic fields are roughly antiparallel. For IMF angles of 90 or 45 degrees, on the other hand, the merging process becomes progressively more concentrated in localized regions near nulls in the magnetic cusps. For a significant fraction of the field lines at the latter two smaller IMF angles, however, the distribution of magnetic reconnection in the simulations clearly extends beyond that inferred from topology merging alone. This is because the topology transition is sometimes preceded by, or takes place in concert with, a second type of reconnection, which typically occurs closer to the subsolar region and is essentially a three-dimensional form of guide field reconnection. This second reconnection process fits the description of "general magnetic reconnection" as described by *Schindler et al.* [1988] and *Hesse and Schindler* [1984] or "virtual field line motion" as described by *Priest et al.* [2003]. Usually this process initially mediates the reconnection of solar wind field lines with each other and then later couples with the topology merging process, leading to simultaneous reconnection at multiple points on the same field line. This phenomenon is exhibited mainly by a subset of field lines at the smaller IMF clock angles that pass close to the magnetic nulls in both the Northern and Southern Hemispheres, regions where, typically, the frozen in condition is strongly violated. Further studies are needed to quantify the importance of this reconnection process elsewhere on the magnetopause, where it may lead to reconnection within, rather than between, the four magnetic topology classes noted earlier.

[4] The complex, spatially distributed nature of reconnection, at least for smaller IMF clock angles, may partially account for why the relative roles of antiparallel versus "guide field" or "component" reconnection at the magnetopause, despite years of research and numerical simulations, has remained a matter of debate. One hypothesis [e.g., *Crooker*, 1979; *Luhmann et al.*, 1984] is that reconnection strongly favors an antiparallel magnetic geometry and is thus mainly prevalent in regions where the solar wind magnetic field is nearly antialigned with the Earth's stretched dipole field. In solar wind orientations without a strong southward component, reconnection is therefore mainly limited to the cusp regions and is absent or infrequent in the vicinity of the subsolar point. Another widely held view [e.g., *Sonnerup*, 1974] is that the reconnection process at the magnetopause is more broadly distributed, with a rate that depends on various factors such as the local shear angle θ_s between the IMF and the Earth's dipole field, the asymmetry in the density and magnetic field profiles across the magnetopause [e.g., *Cassak and Shay*, 2007], and possibly other factors. According to the LFM simulations studied here both of these points of view have merit; most of the magnetic flux that undergoes topology merging does so in regions of nearly antiparallel reconnecting fields. However, the breakdown of the frozen-in condition across the subsolar region leads to guide field reconnection that is more broadly distributed.

2. Reconnection Rates in Two Dimensional Systems

[5] The reconnection rates presented later in this article are computed using three different methods. In this section based on the arguments of the review paper [*Vasyliunas*, 1984] we briefly review the definitions of these three rates and how they are related in a simple two-dimensional system. We show that they should be exactly equal under two idealized assumptions: (1) perfectly time-steady conditions and (2) $E_{\|} = 0$ everywhere except in the immediate vicinity of the separator line. In the global simulations to be discussed later these assumptions are only approximately satisfied and thus the agreement between the three reconnection measures is not perfect.

[6] Consider the antiparallel reconnection geometry shown in Figure 1. A separatrix surface formed by field lines just after they reconnect is shown in gray, bounded by two newly reconnected field lines (red) and a field line drawn from a plasma element just upstream of the surface (blue). In the three-dimensional magnetospheric application of interest, the length of the corresponding separatrix surface, as well as the total amount of reconnected flux per unit time, is finite. Thus the limits of the surface, which are denoted in Figure 1 by the red lines and in the three-dimensional system are determined numerically by field line

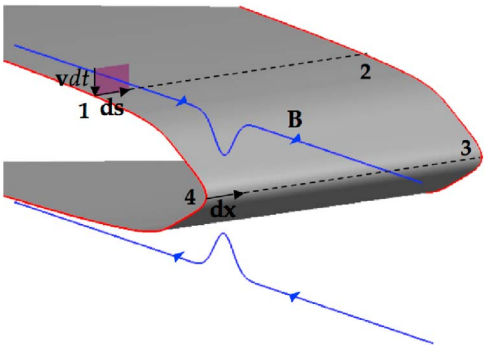

Figure 1. A two-dimensional reconnection geometry with a separatrix surface (gray) formed by field lines just after they reconnect. In the text we refer to a closed loop bounded by two field lines (red), joined by a segment $1 \rightarrow 2$ and a segment of the separator line $3 \rightarrow 4$.

tracing, should be regarded as fixed by the magnetic geometry. When plasma flows across the separatrix surface, the flux tubes embedded in the plasma flow will reconnect. The cross-sectional area of fluid that flows past the separatrix in some time dt is

$$\mathbf{dA} = \mathbf{ds} \times (-\mathbf{v}dt) = \mathbf{v}dt \times \mathbf{ds} \tag{1}$$

where **ds** is a small displacement vector on the separatrix. Therefore the magnetic flux contained in the fluid flowing past the surface is simply $d\Phi = \int \mathbf{B} \cdot \mathbf{dA}$ so that

$$\frac{d\Phi}{dt} = \int_{1\rightarrow 2} \mathbf{B} \cdot (\mathbf{v} \times \mathbf{ds}) = -\int_{1\rightarrow 2} (\mathbf{v} \times \mathbf{B}) \cdot \mathbf{ds} \tag{2}$$

This illustrates the first of three methods methods we use to compute the reconnection rate, a direct computation of the magnetic flux per unit time crossing the separatrix surface.

[7] The flow of plasma in the magnetic field creates potential differences along the separatrix, and we can connect these voltages to the rate at which flux crosses this surface. If we assume that this reconnecting system has reached a steady state, then the magnetic field will be constant in time, $\partial\mathbf{B}/\partial t = 0$, and the electric field will be electrostatic so that $\mathbf{E} = -\nabla\phi$. The magnitude of the potential drop across the separatrix is therefore

$$\Delta\phi = \int_{1\rightarrow 2} \mathbf{E} \cdot \mathbf{ds}. \tag{3}$$

Assuming Ohm's law is ideal so that $\mathbf{E} = -\mathbf{v} \times \mathbf{B}$ this is equivalent to

$$\Delta\phi = -\int_{1\rightarrow 2} (\mathbf{v} \times \mathbf{B}) \cdot \mathbf{ds} \tag{4}$$

Therefore the potential drop along the separatrix is equal to the rate found earlier:

$$\Delta\phi = \frac{d\Phi}{dt}. \tag{5}$$

In the magnetospheric case, the corresponding red field lines are traced numerically down to their endpoints on the Earth's polar cap, and the potential difference between these points thus provides a second, often-used measure of the reconnection rate.

[8] Finally, using Faraday's law, we show that the rate at which flux crosses the separatrix surface is also equal to the integral of the electric field along the separator line (also called the x-line in two-dimensional geometries, here, the line $3 \rightarrow 4$). Consider the loop that bounds the separatrix connecting the labeled points one, two, three, and four. The loop consists of the segment $1 \rightarrow 2$, portions of the two bounding field lines, and the segment along the separator line $3 \rightarrow 4$. Since we have assumed a steady state reconnection geometry, the net change in flux through this surface is zero, and hence by Faraday's law:

$$\int_{1234} \mathbf{E} \cdot \mathbf{dl} = \frac{d\Phi_{1234}}{dt} = 0. \tag{6}$$

Furthermore, if we assume that Ohm's law is ideal along the field line segments $2 \rightarrow 3$ and $4 \rightarrow 1$ then $\mathbf{E}_{\|} = 0$ there and

$$\int_{1234} \mathbf{E} \cdot \mathbf{dl} = \int_{1\rightarrow 2} \mathbf{E} \cdot \mathbf{ds} + 0 \int_{2\rightarrow 3} \mathbf{E} \cdot \mathbf{dl} - \int_{3\rightarrow 4} \mathbf{E} \cdot \mathbf{dx} + 0 \int_{4\rightarrow 1} \mathbf{E} \cdot \mathbf{dl} = 0 \tag{7}$$

$$\Rightarrow \int_{3\rightarrow 4} \mathbf{E} \cdot \mathbf{dx} = \int_{1\rightarrow 2} \mathbf{E} \cdot \mathbf{ds} = \Delta\phi. \tag{8}$$

Therefore by our previous result

$$\int_{3\rightarrow 4} \mathbf{E} \cdot \mathbf{dx} = \frac{d\Phi}{dt}, \tag{9}$$

and so the rate at which flux crosses the separatrix should also be equal to the integral of the electric field along the separator line, our third and final measure of the reconnection rate.

3. Simulation Results

3.1. Parameters

[9] The LFM global magnetospheric simulation code [*Lyon et al.*, 1999] used in this study is based on the equations of ideal magnetohydrodynamics. Although no explicit resistivity is added to the code, diffusion is introduced by numerical effects, which become strong when magnetic field gradient scale lengths approach the computational grid size. The LFM grid is nonuniform, with an average cell size varying from approximately $(\frac{1}{2}R_E)^3$ to $(\frac{1}{4}R_E)^3$ in the magnetopause region of interest. We used constant solar wind conditions with a velocity of 400 km/s in the negative GSM X direction, a density of 6.5 cm^{-3}, and magnetic field strength of 5 nT directed at an Earth with zero magnetic dipole tilt. We performed these simulations for IMF clock angles of 0, 45, 90, 135, and 180 degrees.

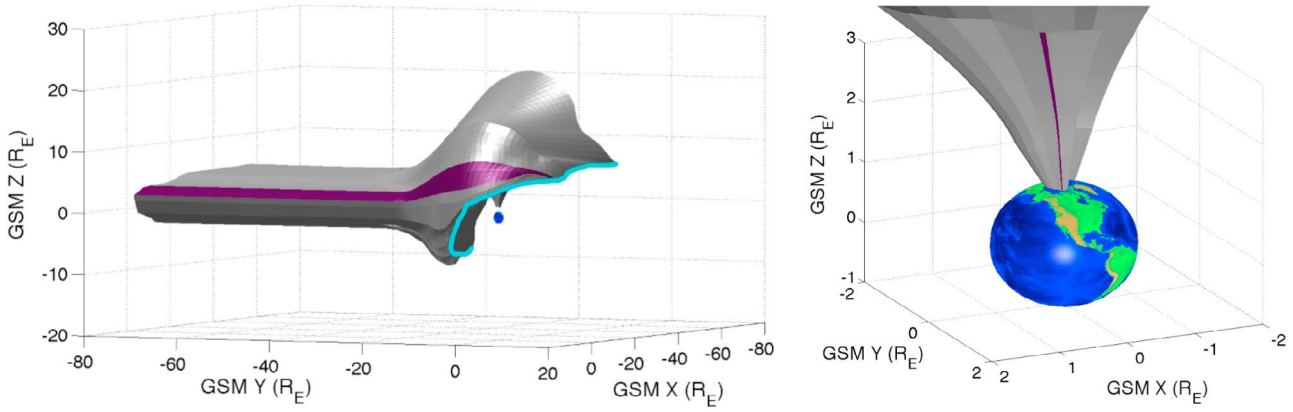

Figure 2. Several important elements of the dayside reconnection geometry for 90 degree (due eastward) IMF conditions. The main plot shows the westward IMF/Open separatrix surface and separator line highlighted in cyan. Field lines lying just in front of the surface are solar wind field lines, and those lying on or just beyond the surface are open field lines with one foot point on the Earth. For visual simplicity, the eastward separatrix has been removed, and the separator line forms the boundary between these two surfaces. The purple stripe of the separatrix is bounded by two newly reconnected field lines. As described in section 2, when plasma flow carries flux across this portion of the separatrix it creates a potential difference between the field lines that bound that segment. If the field lines are well-described as equipotentials, then this potential drop will be equivalent to the integral of $\mathbf{E} \cdot \mathbf{dl}$ along the segment of the separator line connecting these two field lines, and also the potential drop along the portion of the polar cap bounded by these field lines, as can be seen on the right. Summing the individual potential drops across all such segments of the separatrix surface should give us the total reconnection rate, which is equal to both the integral of $\mathbf{E} \cdot \mathbf{dl}$ along the whole separator line and the potential drop across the polar cap.

Each simulation was initialized with a 2 h period of southward IMF followed by a 2 h period of northward IMF and then the final IMF orientation. For our analysis we used data at seven half-hour intervals from 0600 UT to 0900 UT, i.e., 2 h after final IMF onset until the end of the simulation.

3.2. Identifying Global Topology

[10] The first step in our study of magnetopause reconnection was to locate the class of incoming solar wind field lines that had just undergone reconnection at some moment in time, lying just beyond the IMF/open separatrix boundary. For a given moment in time of the simulation, we plotted a dense array of streamlines using the plasma velocity. We traced the streamlines from two lines of very finely spaced points just upstream of the magnetopause and running orthogonal to the direction of the magnetic field in the solar wind. As an example, for 90 degree IMF the streamlines were traced from two lines with $0.04R_E$ spacing oriented parallel to the GSM Z axis and intersecting the X-Y plane at the points ($15R_E$, $\pm 75R_E$, $0R_E$). In the region of space through which the streamlines travel, the solar wind velocity is constant and almost entirely directed in the negative GSM X direction. Therefore the two sets of streamlines originating from these points form two planes normal to the solar wind magnetic field that extend along the direction of solar wind flow. These surfaces, like the velocity field in this region of space, are essentially constant in time. Our goal was to determine all the points where this plane crossed the IMF/open separatrix boundary. To do so we traced magnetic field lines from each point along the streamlines and recorded the topology as an IMF field line with no foot points at the computational grid's inner boundary (e.g., here, the polar cap) or as an open field line with one foot point at the grid's inner boundary. When this topology changed from IMF to open for consecutive points along a streamline we concluded that the streamline had crossed the separatrix boundary. Repeating this process for all the streamlines gave us a large set of points that bracketed the IMF/open separatrix. Convergence was checked by repeating this process with progressively finer resolution both along the streamlines and within the field line tracer module. In Figure 3 we have traced all the field lines that lie just beyond this separatrix and colored them according to topology; open field lines that terminate at the north geographic pole are blue and those that terminate at the south geographic pole are red. The orange line that falls between these two topologies is the separator line. Figure 3 provides a clear snapshot of the global magnetic geometry at a given moment in time.

3.3. Total Dayside Reconnection Rate

[11] This complete set of newly reconnected field lines form a separatrix surface analogous to the simple case of two-dimensional antiparallel reconnection discussed previously. In Figures 2 and 3 we see the magnetopause configuration for 90 degree (due eastward) IMF, showing for clarity just the portion of the surface formed by field lines that eventually terminate on the northern polar cap. As in Figure 1, the separatrix surface is shown in gray, now with a purple stripe highlighting a region of the surface bounded by two typical field lines. By the same reasoning as in the two-dimensional case, under ideal conditions the amount of flux

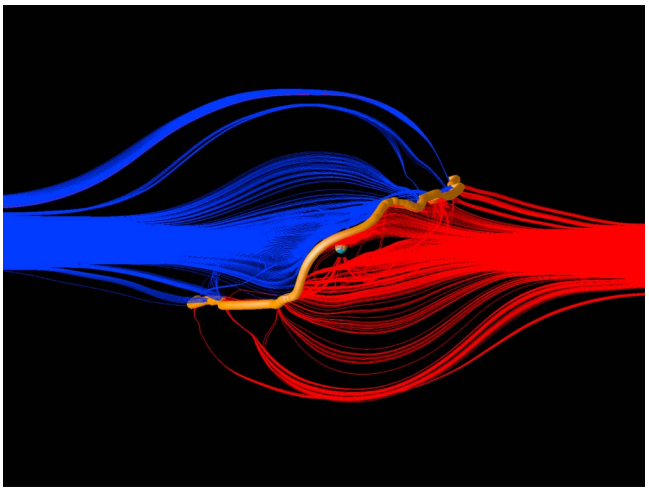

Figure 3. Magnetic skeleton formed by open field lines lying just beyond the IMF/open separatrix in the solar wind for 90 degree IMF. Field lines colored blue connect to the north geographic pole, field lines colored red connect to the south geographic pole, and the orange contour is the separator line. The point of view is from a point on the Sun-Earth line (GSM Z is up; GSM Y is to the right).

crossing the surface per unit time should equal the integral of $E_{\|}$ along the separator line :

$$\Delta\phi = \int_S \mathbf{E} \cdot \mathbf{dl} \tag{10}$$

where S denotes the separator line contour. This is a dayside reconnection rate commonly quoted in the literature [e.g., *Siscoe et al.*, 2001; *Dorelli and Bhattacharjee*, 2008]. Similarly, this rate should also equal the potential difference between the field lines that bound the separtrix surface. As emphasized by *Siscoe et al.* [2001], this potential difference can be conveniently evaluated at the endpoints of the field lines on the polar cap and is typically comparable to the maximum cross-polar-cap potential difference.

[12] Figure 4 shows the total dayside reconnection rates obtained from the three measures as a function of the IMF clock angle. Measurements were taken at half-hour intervals from 0600 UT to 0900 UT and then averaged, with the maximum and minimum values delimiting the error bars. As noted earlier, perfect agreement between the three rates is expected only given a number of idealized assumptions that are not exactly satisfied in the simulations, for example, that the field lines (aside from the separator) are equipotentials. In any case the three rates in most cases are at least roughly comparable and exhibit similar trends, growing roughly linearly from 45 to 135 degrees with more modest increases from 0 to 45 degrees and from 135 to 180 degrees.

3.4. Reconnection Rate Scaling

[13] The solar wind dayside reconnection rate shown as the upper curve in Figure 4 is, by definition, the total amount of solar wind magnetic flux that impinges upon the separator line per unit time. In this section, following ideas similar to those suggested for example by *Kan and Lee* [1979], we describe how to estimate this flux as a function of the IMF clock angle. In Figure 6 we show a set of newly reconnected field lines for IMF angles of 45 and 135 degrees. As the angle of the solar wind increases, the orientation of the line along which reconnection occurs, the separator line, labeled $2R_{MP}$, changes. The separator line transitions from nearly vertical for a 45 degree clock angle to nearly horizontal for a 135 degree clock angle. The angle between the solar wind magnetic field and the separator line also changes. For small IMF angles the separator line differs only slightly in orientation from the solar wind magnetic field, while for large IMF angles they are approximately normal to each other. The separator line thus presents an effective length denoted by $L_{\perp}$ that is perpendicular to the solar wind magnetic field. As θ_{IMF} increases, $L_{\perp}$ also increases, as does the total amount of solar wind magnetic flux per unit time that impinges upon separator line. To a first approximation, this suggests an estimate for the reconnection rate

$$\frac{d\Phi_{sep}}{dt} = C_0 * B_{IMF} v_{sw} L_{\perp} \tag{11}$$

where $C_0 = 0.78$ is a constant of order unity that, for convenience in the plots, has been chosen to yield exact agreement with the simulations data in the southward case ($\theta_{IMF} = 180$). Since B_{IMF} and v_{sw} are the same for all the clock angles, the only factor that varies in equation (11) is $L_{\perp}$. As can be seen from Figure 6, the estimate $d\Phi_{sep}/dt$, excluding for the moment the singular limit of $\theta_{IMF} \rightarrow 0$ (discussed below), yields surprisingly good agreement with the simulations. The values of $L_{\perp}$ upon which this curve are based are obtained from the dipole superposition model, which for the clock angles of 45, 90, 135, and 180

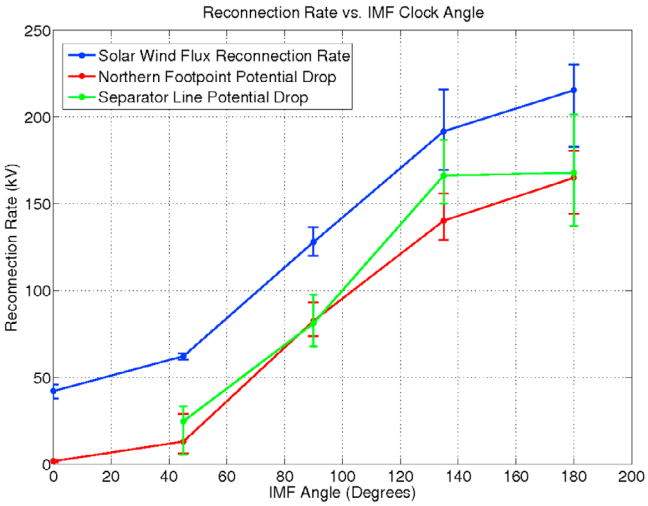

Figure 4. Reconnection rates versus IMF clock angle calculated with three methods, the total amount of flux reconnected in the solar wind (blue), the integral of $\mathbf{E} \times \mathbf{dl}$ along the separator line (green), and potential drop between field lines at the polar cap (red). Owing to the topological instability of northward IMF conditions with zero dipole tilt, we were unable to identify a suitable separator line contour along which to integrate; however, we were able to calculate the other two measures of the reconnection rate.

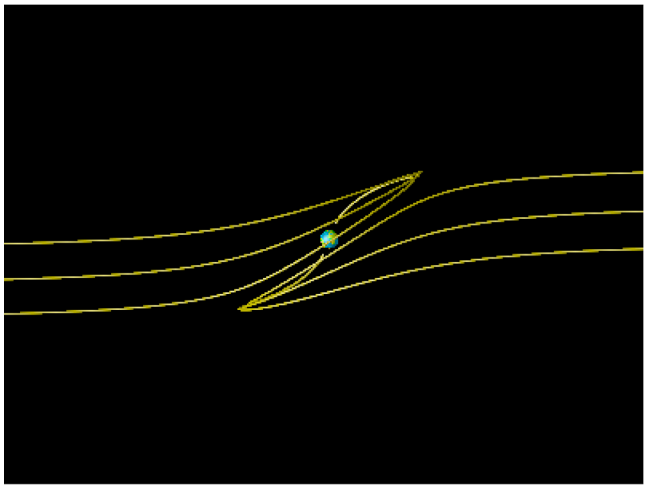

Figure 5. A set of magnetic field lines traced in the dipole superposition model, where we add a constant solar magnetic field to the dipole field of the earth ($\mathbf{B_{Tot}} = \mathbf{B_{Dipole}} + \mathbf{B_{IMF}}$). The dayside magnetic field in this model is qualitatively similar to that of the real magnetopause.

yield good agreement with the values measured directly from the simulations. In the dipole superposition model [e.g., *Lau and Finn*, 1990], the dayside magnetic field is approximated as the sum of a constant solar wind magnetic field and a vacuum dipole field (i.e., $\mathbf{B_{Tot}} = \mathbf{B_{Dipole}} + \mathbf{B_{IMF}}$). This combined magnetic field has the same four magnetic topologies that are found in the actual magnetosphere, and they all meet along a separator line that is comparable in shape to the merging line at the dayside magnetopause (Figures 5–7). The separator line connects two nulls at the dawnside and duskside of the magnetopause, the positions of which correlate well with our simulation data.

[14] As the IMF clock angle approaches due northward ($\theta_{IMF} \rightarrow 0$), the separator line becomes progressively more parallel to the IMF field, and thus both $L_\perp$ and the reconnection rate predicted by equation (9) go to zero. This is in contradiction with the simulations, which exhibit only a weak drop in the reconnection rate as θ_{IMF} falls below 45 degrees. However, as will be discussed in the next section, the orientation of the separator line is not the only factor that governs the spatial distribution of reconnection in the simulations; the strength of the local magnetic field also plays a key role. Strong topology merging in the simulations for a given clock angle, as we discuss later, is observed to be mostly confined to within regions of weak $|\mathbf{B}|$ along or near the separator, for example, regions in which the magnetic field strength falls below approximately half the magnetosheath field strength, here about 10 nT or less. At IMF clock angles of 135 degrees and larger, this condition is met along the entire separator line, consistent with the broad distribution of topology merging observed at these large clock angles. As θ_{IMF} falls below about 90 degrees, on the other hand, the weak $|\mathbf{B}|$ regions become more and more localized to the vicinity of the two nulls in the magnetic cusps. In the near-northward IMF limit, as shown in Figure 8, these regions approach two localized patches surrounding the poles on the magnetopause with a width of roughly $L_0 \sim 5.5R_E$ in the GSM Y direction. Replacing $L_\perp$ in our scaling law $d\Phi_{Sep}/dt$ by L_0, we obtain a value of the reconnection rate for $\theta_{IMF} = 0$ (see Figure 9) that is in good agreement with the simulations. This indicates that essentially all of the solar wind magnetic flux that flows into these weak $|\mathbf{B}|$ zones of width $\sim L_0$ undergoes reconnection, similar to the situation at larger clock angles aside from $L_0 \rightarrow L_\perp$. It should be noted that this value of L_0 can change depending on what specific magnetic field threshold is used. For example, we found that increasing this threshold to $15nT$ increased L_0 to $9R_E$ whereas decreasing the threshold to $5nT$ decreased L_0 to $2R_E$.

[15] The dependence of $L_\perp$ and thus $d\Phi_{sep}/dt$ on θ_{IMF} in the simulations is similar some other scaling laws that have been presented in the literature. As shown in Figure 6:

$$L_\perp = 2R_{MP}\sin(\theta) = 2R_{MP}\sin(\theta_{IMF} - \theta_n), \qquad (12)$$

where θ_n is the polar angle of the nulls that set the orientation of the separator line and R_{MP} is the radius of the

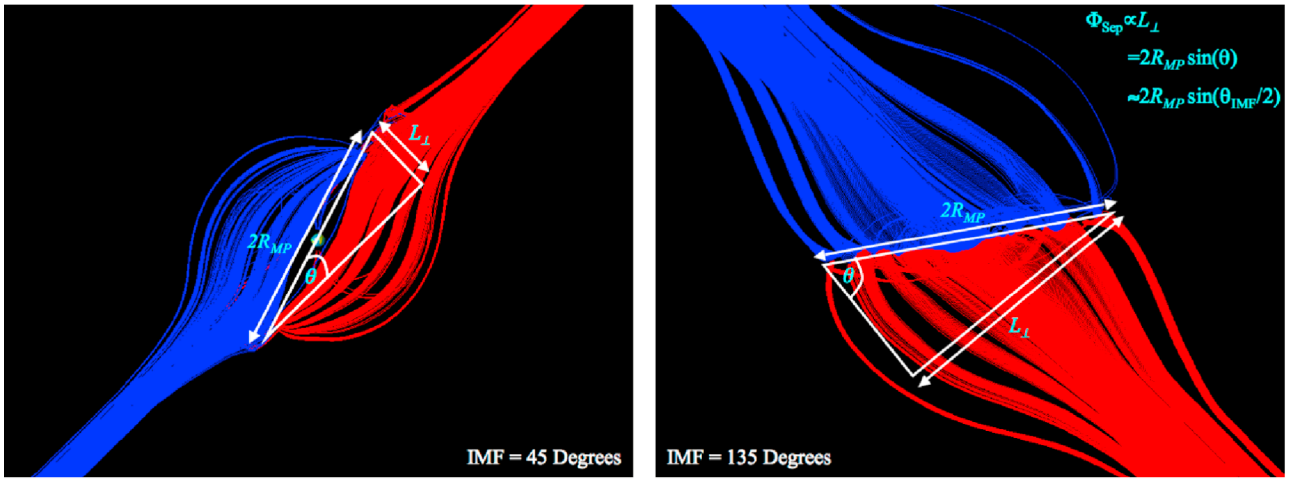

Figure 6. Φ_{Sep} for different IMF clock angles. As the angle of the separator changes relative to the solar wind magnetic field, more magnetic flux encounters the separator line. The scaling of this flux with IMF angle largely matches that of the dayside reconnection rate.

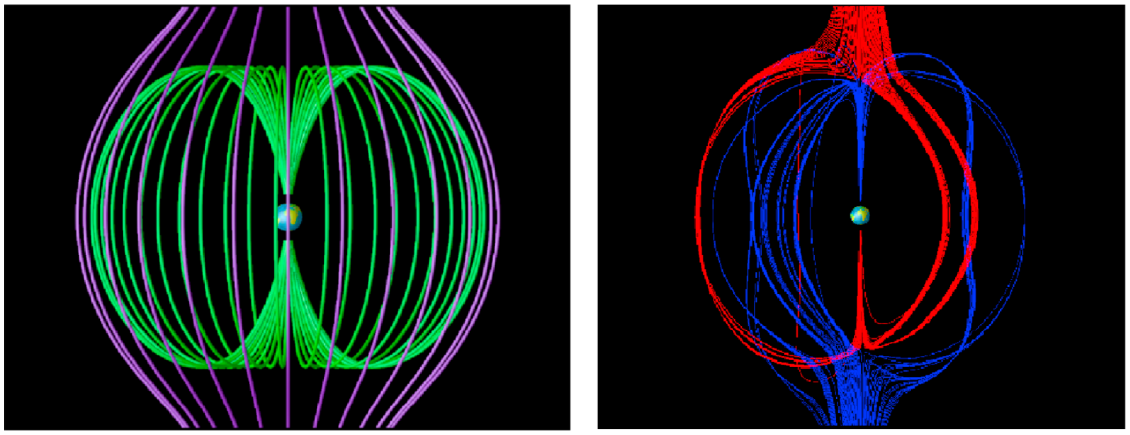

Figure 7. Magnetopause topology predicted by (left) the dipole superposition model and (right) simulation results for northward IMF conditions. In the dipole superposition model, only a singular field line that runs through geomagnetic dipole axis will reconnect; hence the reconnection rate is zero. In contrast, we observe that some finite amount of flux is reconnected under northward IMF conditions. We determined that this rate can be roughly estimated by the size of the weak |**B**| region on the magnetopause where reconnection occurs.

magnetopause in the GSM X = 0 plane. To within 10 degrees, the position of these nulls in our model is approximately $\theta_{IMF}/2$ (a property noted by *Kan and Lee* [1979]) so that

$$L_{\perp} \simeq 2R_{MP}\sin(\theta_{IMF}/2). \quad (13)$$

With this expression for $L_{\perp}$, one obtains the green curve in Figure 6. Many predictions of the dayside reconnection rate in the literature contain a factor of $\sin^n(\theta_{IMF}/2)$ [see, e.g., *Newell et al.*, 2007; *Perrault and Akasofu*, 1978; *Vasyliunas et al.*, 1982; *Scurry and Russell*, 1991; *Temerin and Li*, 2006].

3.5. Local Reconnection Metrics

[16] In a previous section we characterized the total rate of reconnection at the dayside magnetopause. We now turn to the questions of where and in what form the reconnection actually takes place. To do this we again apply three different methods, described in this section, to our field line dataset. In most cases the results from the three measures overlap, providing some measure of confidence that reconnection has indeed been located.

[17] The first method examines the motion of the solar wind field lines and plasma just prior to and during the topology transition, looking for the locations where the field lines and plasma decouple. To do this we developed a parameter called $d_{\perp}$, for "perpendicular distance." Consider a solar wind fluid element flowing toward the Earth in a region in which the frozen-in law is well satisfied. At two slightly different times, t_0 and t_1, a field line embedded in this fluid element is traced toward the Earth, as shown

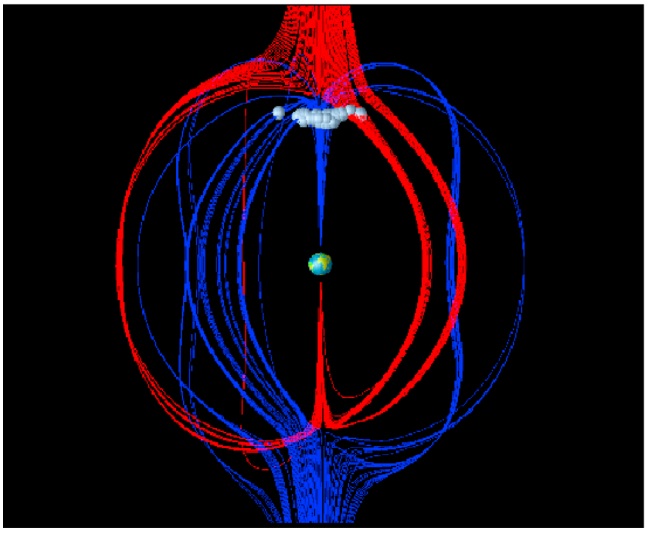

Figure 8. Magnetic skeleton for northward IMF conditions. The gray spheres denote weak B regions whose width we used in our scaling law $d\Phi_{Sep}/dt$.

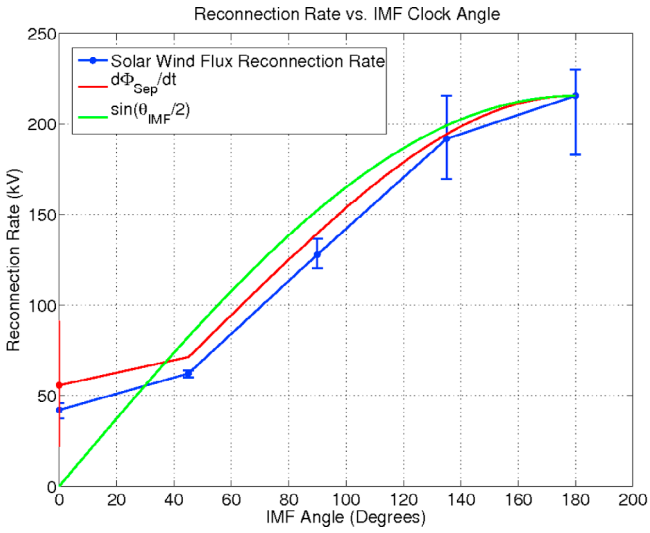

Figure 9. A comparison of the measured dayside reconnection rate and the estimate $d\Phi_{Sep}/dt$ given by equation (11). For the due northward IMF case, we measured the width of the reconnection region L_0 to be between 2 and 9 R_E.

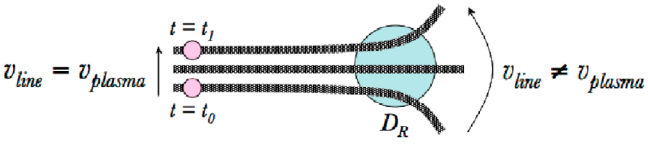

Figure 10. Example of virtual field line motion. The field line is traced from a fluid element convected with the plasma velocity on the left side of a diffusion region (blue circle). It then continuously changes its magnetic connectivity, creating a "virtual" motion on the right side of the diffusion region. (based upon Figure 7 in the work of *Priest et al.* [2003]).

schematically in Figure 10. At many points along the first field line (traced at time t_0) we calculate the perpendicular distance to the second field line (traced at time t_1) and then normalize this distance to the local perpendicular plasma velocity $v_\perp$ times the time interval $dt = t_1 - t_0$. As long as the field line travels through a region in which the frozen-in condition is well satisfied, the local perpendicular displacement from the first field line to the second should be equal to the corresponding displacement of the local fluid elements $v_\perp * dt$, and hence the value of $d_\perp$ should be unity. However, when a field line passes through a diffusion region its motion decouples from the plasma velocity and we observe a perpendicular displacement between the field lines that typically exceeds $v_\perp * dt$ so that $d_\perp$ becomes much larger than one. A demonstration of how $d_\perp$ behaves for two field lines from our data set is shown in Figure 11. As the field lines enter a diffusion region where reconnection occurs they diverge rapidly, indicated by a sudden increase in $d_\perp$. This method is designed to capture reconnection that fits the broader definition advocated by *Hesse and Schindler* [1984] and *Schindler et al.* [1988]. One of its strengths is that it can identify reconnection of all forms, including those involving only field lines within the same topological class.

[18] The second method is topological and attempts to identify likely reconnection sites based on where field lines of different topologies intersect. In magnetopause reconnection, as shown for example by Figure 11, solar wind field lines merge with closed, dipolar field lines to create field lines with one foot point on the Earth and the other in space. The closed field line in Figure 11 was traced from a point slightly lower in latitude from where the open field line encounters the polar cap. This method determines where these field lines meet along the separator line, since this line is by definition the locus along which the topologies of magnetic field come together. Although such a conjunction of topologies might in principle occur even in an ideal plasma, in practice these locations are clearly sites where the frozen-in condition is significantly broken, as we show later.

[19] The third method considers the spatial distribution of a normalized measure of the frozen in law, and the identification of regions where this condition is strongly violated. This method is based on a dimensionless parameter *DE* that measures the degree to which the plasma is frozen-in:

$$DE = \frac{|\mathbf{E} + \mathbf{v} \times \mathbf{B}|}{|\mathbf{E}| + |\mathbf{v} \times \mathbf{B}|}. \quad (14)$$

[20] If *DE* is close to its minimum value of zero in some region, then Ohm's law is nearly ideal and the frozen-in condition is well satisfied there. However, when *DE* approaches its maximum value of one, it indicates the presence of strongly nonideal behavior. A weakness of this measure is its insensitivity to reconnection with a strong guide field component, since in this case the reconnection terms in Ohm's law are typically small compared to those associated with $\mathbf{E} \times \mathbf{B}$ convection of the guide field.

[21] It is important to note that the type of metrics employed can have an effect on where reconnection is identified. Other simulations such as those by *Dorelli et al.* [2007] that employ explicit resistivity have used the quantity ηJ as a way to determine where reconnection is occurring and have obtained results concerning the distribution of reconnection that are different than ours. Since our simulations do not contain an explicit resistivity of this form, we have chosen not to employ this measure in our study. This choice of metrics may be one reason why we reach the specific conclusions we do regarding the type and distribution of reconnection in our simulations.

3.6. Reconnection Processes

[22] When we combine these three methods, we are presented with two different reconnecting processes. In the most common form of reconnection all three methods overlap; $d_\perp$ diverges rapidly in a region of strong magnetic diffusion, as identified by *DE*, very close to the location of topology merging on the separator line. Field lines enter these regions of strong magnetic diffusion where the closed, open, and solar wind magnetic field topologies join together and we observe a rapid change in the shape of the field lines within this region. In Figure 13 we have colored the mag-

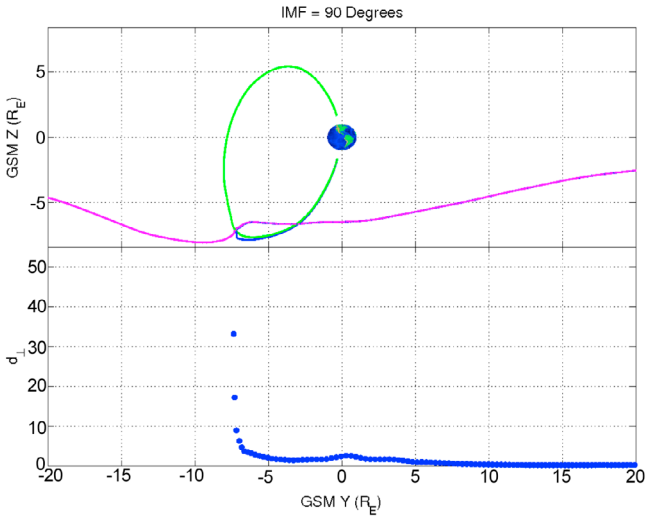

Figure 11. An example of how the parameter $d_\perp$ varies along a field line. This parameter is the distance perpendicular to **B** from the purple IMF field line to the blue open field line, normalized to the displacement we would expect from the local perpendicular plasma velocity $v_\perp$. When the frozen-in condition is satisfied, the field lines are separated by a distance equal to the distance of plasma flow and so $d_\perp$ is equal to unity. When the field line enters the strong diffusion region at $Y = -7R_E$ we observe $d_\perp$ diverging rapidly.

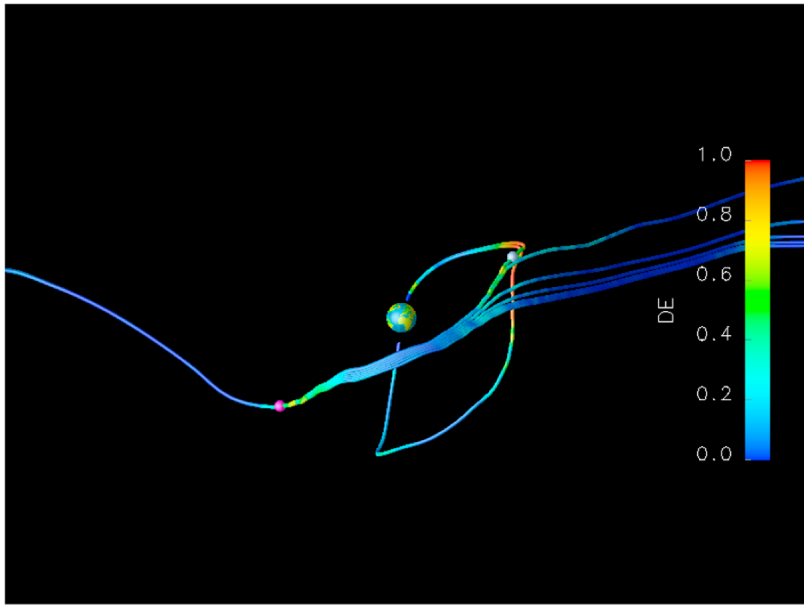

Figure 12. Example of a reconnection geometry in which the frozen-in condition breaks down in a location separate from where the topologies come together. The magenta dot marks where the frozen-in condition breaks down, and the gray dot marks the location of topology merging. The field lines are colored with *DE*, where regions shaded red indicate large magnetic diffusion and regions colored blue indicate low magnetic diffusion. The image's viewpoint is from a position just above the Sun-Earth line (GSM Y is still to the right).

netic skeleton formed by the newly reconnected open field lines with the DE parameter and mark the locations where we find topology merging with gray spheres. We can see that these reconnection sites tend to cluster in areas of strong magnetic diffusion, as indicated by large *DE* values. The fact that the locations where we identify topology merging lie within regions of strong magnetic diffusion gives us an indication that reconnection is indeed taking place in these regions.

[23] In the second type of reconnection process, regions of strong magnetic diffusion, as indicated by *DE* and $d_{\perp}$, can be encountered by a field line prior to, and in regions spatially distant from, the topology merging point. An example is shown in Figure 12. In this picture we see the evolution of a solar wind field line just before reconnection, the open field line just after the reconnection event, and the closed field line that lies just below the polar cap boundary near the open field line. The field lines are colored with the diffusion parameter *DE*. Clearly, the magnetic field ceases to be frozen into the plasma flow at a point on the southern dawnside of the magnetopause, while the place where the topologies come together is located on the northern duskside. Furthermore, both of these places are regions of strong magnetic diffusion, as identified by *DE*. We only observed this process for IMF clock angles of 45 and 90 degrees, with the breakdown in the frozen-in condition originating in mainly two regions of strong magnetic diffusion at the northern duskside and southern dayside of the magnetopause, as shown in Figure 13. For these two clock angles this process occurred approximately half as often in our field line data set as the first type of reconnection described above.

[24] This process fits the description of "general magnetic reconnection" as described by *Hesse and Schindler* [1984] and *Schindler et al.* [1988] in which two fluid elements that were initially connected by a field line are no longer magnetically linked at a later time due to the passage of the field line through a diffusion region. One manifestation of this form of reconnection, described for example by *Priest et al.* [2003], is "virtual field line motion". Referring to Figure 10, at several moments in time we trace the magnetic field line tied to a plasma fluid element. When the field line intersects a diffusion region, the frozen-in condition breaks down and it reconnects onto a continuously varying set of new field lines, thus appearing to "flip" at a speed much greater than the plasma velocity on the far side of the diffusion region. In Figure 12 the situation is very similar. The nonclosed field lines shown are traced from points along a velocity streamline that lies to the left of the image's viewable area. The points that we trace the field lines from are spaced so closely together that the resulting contours are indistinguishable until they pass through the diffusion region, yet beyond this region the field lines have a much larger separation. The plasma velocity on either side of these diffusion regions is approximately the same, so the displacements we observe are much larger than plasma convection could produce. This behavior could also be described as merging in the presence of a large guide field. In strongly component reconnection, the magnetic fields would appear to rotate slightly around the reconnection point. This process may be occurring, for example, at the location indicated by the magenta dot in Figure 12. It could also be occurring somewhere further along the field line toward the subsolar point.

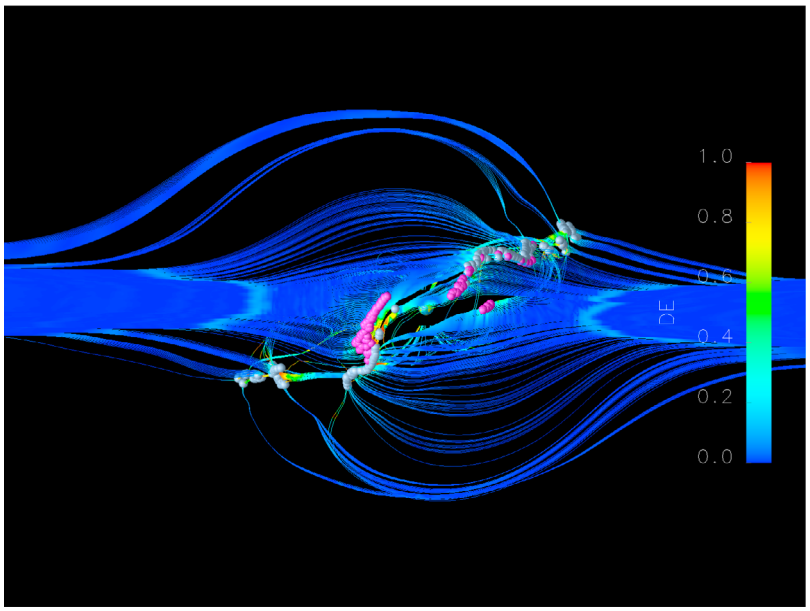

Figure 13. Magnetic skeleton colored with *DE* and showing locations of topology merging (gray dots) and breakdown in the frozen-in condition (magenta dots). Note how both types of reconnection are concentrated in regions where Ohm's law is nonideal, though the topology merging occurs in regions of stronger magnetic diffusion. This image uses the same viewpoint as Figure 3.

[25] In view of the potentially dramatic difference between the motions of the field lines and the plasma, it is important to ask what physics can be learned from field line tracing methods in three-dimensional nonideal plasmas. The virtual field line effect in 3-D is simply a more gradual version of the instantaneous motions made by reconnecting field lines in two-dimensional systems: in 2-D, due to the existence of well-defined flux surfaces, a field line enters a diffusion region and, at some instant of time, breaks and reforms, effectively causing the portion of the field line on the far side of the diffusion region to change its location instantaneously. This effectively infinite field line velocity at the instant of reconnection can be moderated in three dimensions, in which the field lines change their connections over a typically brief but finite period of time (depending on the size of the diffusion region) and the virtual field line speeds observed during this period are correspondingly large but finite. In either case, the reconnection process produces field lines that are kinked to varying degrees depending on the guide field strength, and when these field lines eventually emerge from the diffusion zone and once again become frozen in, their relaxation transforms magnetic energy into kinetic energy of the plasma. This process is expected to have a progressively weaker impact on the plasma as the reconnecting component of the magnetic field, and thus the amount of released magnetic energy, becomes small. On the other hand, if guide field reconnection occurs over a sufficiently large area, its overall impact may be significant.

[26] Another argument against field line tracing methods [*Newcomb*, 1958] is based on an ambiguity that exists even in an ideal plasma. Consider a region of space where the ideal Ohm's law holds and $\mathbf{E} = -\mathbf{v} \times \mathbf{B}$, where $\mathbf{v}$ is the bulk flow velocity. If we introduce a new flow velocity $\mathbf{w}$ that depends on an arbitrary function ψ as $\mathbf{E} = -\mathbf{w} \times \mathbf{B} + \nabla\psi$ then $\mathbf{w}$ is given by

$$\mathbf{w} = \frac{(\mathbf{E} - \nabla\psi) \times \mathbf{B}}{B^2}. \tag{15}$$

If we substitute this new expression for $\mathbf{E}$ into Faraday's law, we find

$$\frac{\partial \mathbf{B}}{\partial t} = \nabla \times (\mathbf{w} \times \mathbf{B} + \nabla\psi) = \nabla \times (\mathbf{w} \times \mathbf{B}), \tag{16}$$

and so the magnetic flux can be regarded as frozen into the (effectively arbitrary) velocity field $\mathbf{w}$, as well as into the plasma velocity $\mathbf{v}$. In the context of an MHD simulation, however, the utility of the frozen-in concept lies in what (if anything) it can teach us about the dynamics of the *plasma* velocity, the only velocity field (in an MHD code) that has physical significance. In the case of magnetic reconnection these dynamics are typically just the energy exchange between magnetic tension and plasma flows, as in the case of an Alfvén wave.

3.7. Local Reconnection Rate and Distribution of Reconnection

[27] There are multiple approaches one can take to measure the local reconnection rate in a region of the magnetopause. One approach is to measure the parallel electric field near the separator line [*Siscoe et al.*, 2001]. One potential problem with this method, however, is that the electric field often has large spatial variance in regions near the separator line, and so a small error in the physical location of the merging line can give an inaccurate measure

of the local reconnection rate. Additionally, even for steady solar wind conditions, time-dependent modes such as Kelvin-Helmholtz waves on the flanks of the magnetopause can give rise to electric fields that either reduce or enhance the reconnecting electric field [*Claudepierre et al.*, 2008]. These drawbacks can be avoided by relating, as discussed in previous sections, the local parallel electric field on the separator line to the reconnected flux in the solar wind. Consider the simple two dimensional geometry of Figure 1 and assume that the diagram represents a short segment of the separator line. Therefore we can say that the integral of **E** along the separator line is

$$\int_{3\rightarrow 4} \mathbf{E}\cdot\mathbf{dx} = E_{\parallel}dx, \tag{17}$$

where $E_{\parallel}$ is the electric field parallel to the small segment of the separator line dx. However, by our previous results we also know that this potential difference is equal to the rate at which flux crosses the separatrix surface. Therefore we can say that the local electric field along this small segment of the separator line should be

$$E_{\parallel} = \frac{\frac{d\Phi}{dt}}{dx}, \tag{18}$$

i.e., the local parallel electric field is equal to the spatial density of the flux in small reconnected flux tubes. In practice, we can approximate the center of these tubes as field lines and say that the flux contained in a small flux tube around that field line is reconnected where it contacts the separator line. If one repeats this process, tracing out a set of field lines that cover the entire separatrix surface, the distribution of points where these field lines contact the separator line gives us an indication of how the reconnected flux is distributed along the merging line. For example, if most of these field lines traced from the solar wind map down to a narrow region of the merging line, then the flux is being reconnected in a relatively concentrated area.

[28] This topology merging class of reconnection occurs, by definition, along a separator line between magnetic topologies. To determine this contour, we impose a best fit line through the previously determined set of merging points. Using a smoothing spline interpolation scheme, we adjust the fit parameters so that the resulting contour lay in between the two classes of open magnetic field lines (Figure 3). We then assume, as described in our discussion of reconnection rates, that the amount of flux reconnected at the point where each of our newly reconnected field lines encountered the separator was equal to the amount of flux crossing the boundary between IMF and open field lines in the vicinity of this open field line. We then sum the amount of flux reconnected near several segments of the separator line that were equal in length by adding up the amount of flux contained within flux tubes that terminated at the reconnection sites near these separator line sections. Figure 14 shows the resulting plots of the separator lines, using a color scale to express how much flux was reconnected versus position.

[29] When we compare these plots for the four different IMF clock angles, we notice a substantial difference in where topology merging was predominant at the magnetopause. For 45 degree IMF, the reconnection is concentrated in two well defined regions at the northern duskside and southern dawnside of the magnetopause, and does not occur across the subsolar point. For clock angles of 135 and 180 degrees the reconnection extended across the subsolar point and, though not evenly distributed, occurs at more locations along the separator line than for the smallest clock angles. For due eastward (90 degree) IMF, the situation was slightly more complicated. For the first five time slices we examined, representing two hours of simulation time from 0600 UT to 0800 UT, the reconnection was spatially localized in two well defined regions just as with 45 degree IMF. However, for the last two time slices at 0830 UT and 0900 UT, we did observe topology merging across the subsolar point, with approximately 20% and 15% of the total flux reconnected between the northern duskside and southern dawnside regions.

[30] The distribution of the component process for IMF angles of 45 and 90 degrees is correlated with that of the merging process, occurring within diffusion regions that extend in wide swaths from the area around the clusters of topology merging and also along the separator line. In Figure 12, as a field line journeys from the dawnside, the frozen-in condition breaks down in a diffusion region along the southern dawnside, where we have identified flux from the duskside of the magnetopause reconnecting. The interplay of these two reconnecting processes makes general claims about the total distribution of reconnection difficult. The precise way in which the magnetic energy in reconnecting flux tubes is converted to plasma is complicated, occurring over larger swaths of the magnetopause as opposed to specific regions of the separator line.

3.8. Average Magnetic Shear

[31] To classify the topology merging process as antiparallel or component in nature, we also determined the distribution of magnetic shear along the separator line. In a simple two-dimensional reconnection geometry, the shear angle of the magnetic fields is readily attained; one simply compares $\hat{\mathbf{b}}$ on either side of the diffusion region. In the magnetopause context we compute the angle between the local dipole field and the local solar wind field. For all clock angles we found that in the regions where most of the topology merging was concentrated, the magnetic shear angles were large, in excess of 140 degrees. The mean shear angles for various regions of the separator line are shown in Figure 14.

[32] In the 45 and 90 degree clock angle cases, we believe that the magnetic merging can be described as occurring in the vicinity of nulls or clusters of nulls in the magnetic field at the northern duskside and southern dawnside of the magnetopause. There are several observations that lead us to this conclusion. First, as noted previously, the reconnecting fields were strongly sheared, with shear angles in excess of 150 degrees. This indicates the reconnection was primarily an antiparallel process which would produce magnetic nulls. We also observe that $|\mathbf{B}|$ weakened in these regions. Examining a plot of $|\mathbf{B}|$ versus separator line length (Figure 15), we see that in the regions where most of the flux was reconnected the magnetic field became weak, approaching

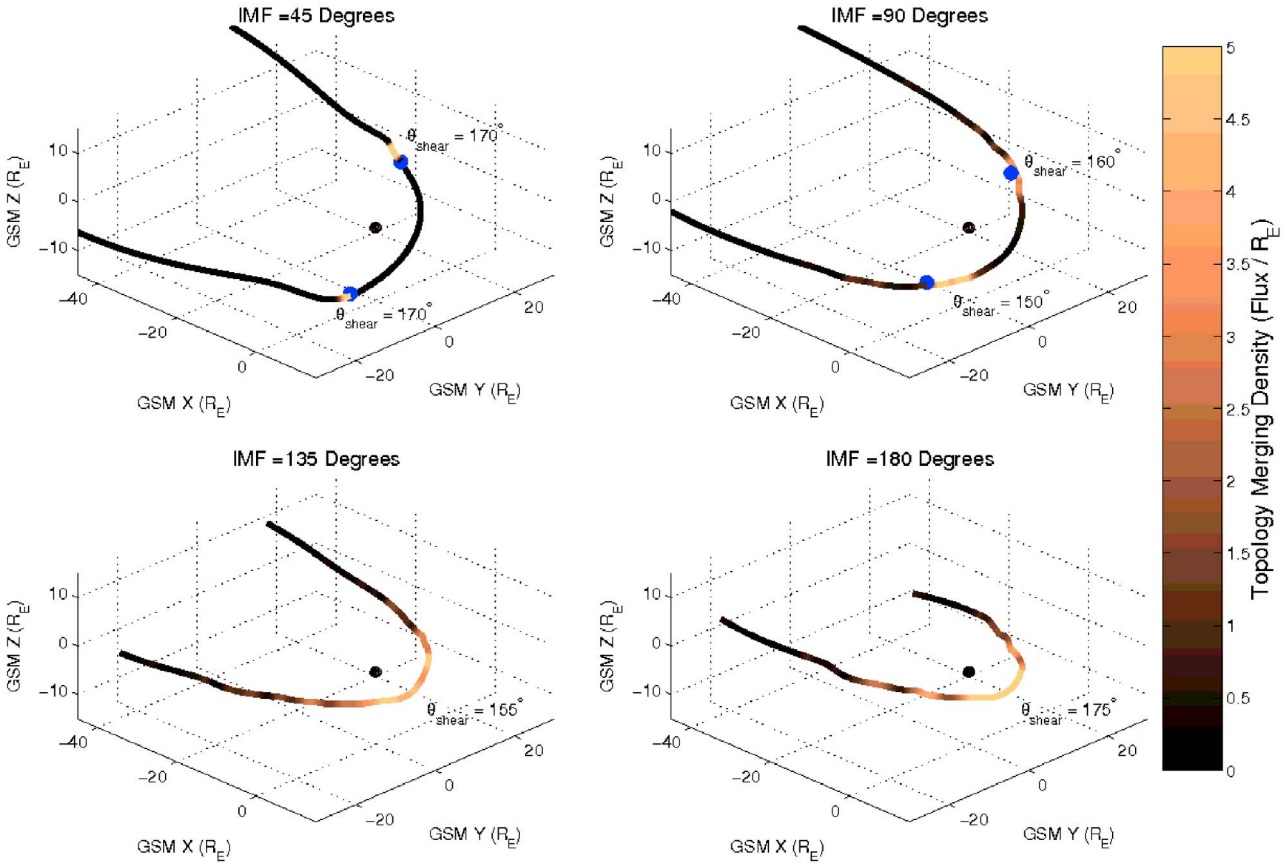

Figure 14. Plots showing how the distribution of topology merging varies with IMF clock angle. We assume that flux from the solar wind was reconnected at each of the points we had identified as a location of topology merging and then summed up the total amount of flux that reconnected within a region of the separator line. The separator lines shown here are averaged using data from all times analyzed 0600 UT to 0900 UT. The color of the line indicates how much topology merging occurs near that part of the separator. Light copper regions indicate where the process is localized; darker colors indicate less topology merging.

values of 1 or 2 nT, easily an order of magnitude below the ambient field in the magnetosheath. Finally, the locations where we observe most of the reconnection occurring are consistent with where we would expect magnetic nulls to form using a dipole superposition model. As mentioned previously, in the dipole superposition model there are exactly two nulls created for all IMF clock angles excluding 180 degrees, and their locations can be calculated analytically. When we plotted these predicted null locations on the magnetopause surface, we found that they were near the sites where we observed most of the topology merging.

[33] As noted earlier, the size of regions in which the magnetic field is weak also appears to play some role in governing the observed distribution of topology merging. When we compared the magnitude of **B** along the separator line to the distribution of merging (Figure 15), we found that as one moves away from the subsolar point (indicated by the peak in |**B**|), the regions of strongest reconnection appear to begin when |**B**| drops below approximately 15 nT. As the IMF angle increases, we noted that these weak |**B**| regions moved closer together, i.e., the reconnection initiated closer to the subsolar point. This trend may explain why the reconnection moves toward and eventually crosses the subsolar point as the IMF clock angle increases.

4. Conclusions and Discussion

[34] In summary, we observe a strong dependence of the distribution and total amount of reconnected flux at the dayside magnetopause on the solar wind clock angle, growing linearly for IMF angles of 45 to 135 degrees and then increasing more modestly from 0 to 45 degrees and from 135 to 180 degrees. This trend may be explained by the trend in flux that impinges upon the separator line, or null region in the case of northward IMF conditions, at the magnetopause with clock angle. From 45 to 180 degree IMF angles we show that this quantity scales as approximately $\sin(\theta_{IMF}/2)$ as noted by *Kan and Lee* [1979]. An important question for future studies is whether these conclusions continue to hold when the grid resolution is refined (and thus the numerical resistivity becomes smaller) or when new physics such as the Hall term in Ohm's law is included.

[35] To probe the local properties of reconnection at the magnetopause, we used three measures, examining how

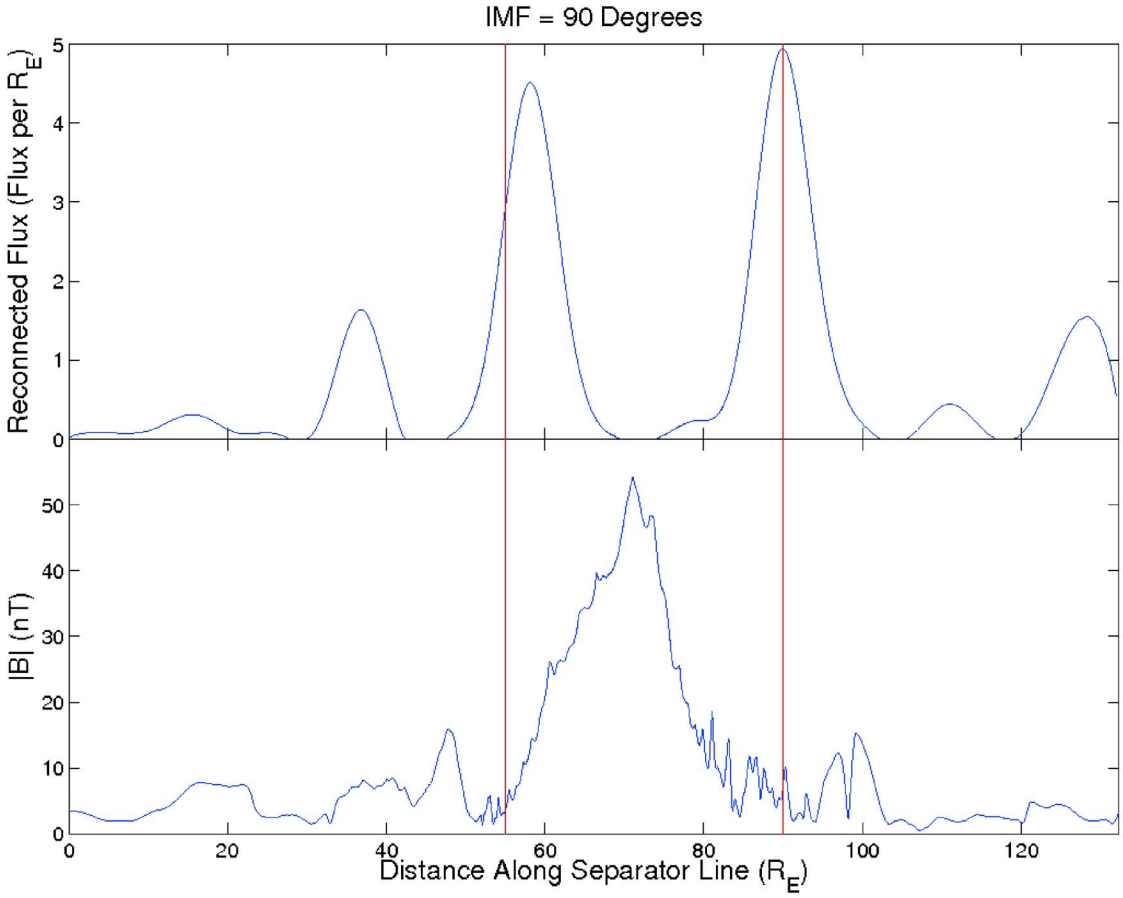

Figure 15. Variation of |**B**| and reconnected flux along the separator line for a 90 degree IMF. Note how the two peaks in reconnected flux density occur near regions where |**B**| has minima on the separator line.

rapidly field lines changed their topology, where different magnetic topologies merged together, and the location of strong magnetic diffusion regions. Using these measures, we identified two distinct reconnection processes at the dayside magnetopause. The first process fits the definition of traditional topology merging reconnection, in which magnetic field lines change from having both foot points in the solar wind to having one foot point at the Earth. For IMF clock angles of 45 and 90 degrees this topology merging occurs primarily in well defined regions of strong magnetic diffusion near the magnetic cusp nulls, while for clock angles of 135 and 180 degrees the reconnection extends across the subsolar point. In both cases the reconnection initiates along the separator line in regions of weak magnetic field, regions that move closer to the subsolar point with increasing IMF angle.

[36] For IMF angles of 45 and 90 degrees, we also observed a reconnection process in which the frozen-in condition first fails in a region removed from where the topology merging occurs. This may be an example of strongly component reconnection and/or the so-called "virtual field line motion" as described by *Priest et al.* [2003]. This process is more broadly distributed around diffusion regions on the magnetopause surface and can occur in conjunction with the topology merging process. The simultaneous occurrence of both component and antiparallel reconnection under conditions where the IMF had a strong east-west component was observed by the Cluster and Double Star missions, as described by *Pu et al.* [2005, 2007]. The coupling of these two processes may convert magnetic energy into plasma energy over a larger area of the magnetopause than would be inferred from the topology merging process alone.

[37] There are several noteworthy limitations of this study. Our analysis is focused mainly on the subset of field lines that undergo topology merging and the behavior of these field lines just before and after the merging process. Our results clearly show however that guide-field-like reconnection can take place independent from topology merging, and thus a more global study of reconnection in all its forms is warranted. We have not examined in detail how the amount and distribution of reconnection depends on factors such as the numerical grid scale, the dipole tilt, and non-MHD physics such as the Hall term in Ohm's law or how the relaxation of field lines is related to plasma flows or the penetration of plasma into the magnetosphere.

[38] **Acknowledgments.** This work was supported by the NSF through its funding of the Center for Integrated Space Weather Modeling (CISM) and by NASA HTP award NNX08AI36G. Much of the field line tracing and visualization was done using the CISM-DX software package [*Wiltberger et al.*, 2005].

[39] Zuyin Pu thanks the reviewers for their assistance in evaluating this paper.

References

Axford, W. I. (1984), Magnetic reconnection, in *Magnetic Reconnection in Space and Laboratory Plasmas*, *Geophys. Monogr. Ser.*, vol. 30, edited by J. E. W. Hones, pp. 1–8, AGU, Washington, D.C.

Boozer, A. H. (1975), Reconnection and the ideal evolution of magnetic fields, *Phys. Rev. Lett.*, *88*, 303–336.

Cassak, P. A., and M. A. Shay (2007), Scaling of asymmetric magnetic reconnection: General theory and collisional simulations, *Phys. Plasmas*, *14*, 102,114.

Claudepierre, S. G., S. R. Elkington, and M. Wiltberger (2008), Solar wind driving of magnetospheric ULF waves: Pulsations driven by velocity shear at the magnetopause, *J. Geophys. Res.*, *113*, A05218, doi:10.1029/2007JA012890.

Crooker, N. U. (1979), Dayside merging and cusp geometry, *J. Geophys. Res.*, *84*(A3), 951–959.

Dorelli, J. C., and A. Bhattacharjee (2008), Defining and identifying three-dimensional magnetic reconnection in resistive magnetohydrodynamic simulations of Earth's magnetosphere, *Phys. Plasmas*, *15*, 056504.

Dorelli, J. C., A. Bhattacharjee, and J. Raeder (2007), Separator reconnection at Earth's dayside magnetopause under generic northward interplanetary magnetic field conditions, *J. Geophys. Res.*, *112*, A02202, doi:10.1029/2006JA011877.

Greene, J. M. (1993), Reconnection of vorticity lines and magnetic lines, *Phys. Fluids B*, *5*, 2355–2362.

Hesse, M., and K. Schindler (1984), A theoretical foundation of general magnetic reconnection, *J. Geophys. Res.*, *93*(A6), 5559–5567.

Kan, J. R., and L. C. Lee (1979), Energy coupling function and solar wind-magnetosphere dynamo, *Geophys. Res. Lett.*, *6*(7), 577–580.

Lau, Y.-T., and J. M. Finn (1990), Three dimensional kinematic reconnection in the presence of field nulls and closed field lines, *Astrophys. J.*, *350*, 672–691.

Luhmann, J. G., et al. (1984), Patterns of potential magnetic field merging on the dayside magnetopause, *J. Geophys. Res.*, *89*(A3), 1739–1742.

Lyon, J. G., J. A. Fedder, and C. M. Mobarry (1999), The Lyon-Fedder-Mobarry (LFM) global MHD magnetospheric simulation code, *J. Astron. Sol. Terr. Phys.*, *66*, 1333–1350.

Newcomb, W. A. (1958), Motion of magnetic lines of force, *Ann. Phys.*, *3*, 347.

Newell, P. T., et al. (2007), A nearly universal solar wind-magnetosphere coupling function inferred from 10 magnetospheric state variables, *J. Geophys. Res.*, *112*, A01206, doi:10.1029/2006JA012015.

Perrault, W. K., and S.-I. Akasofu (1978), A study of geomagnetic storms, *Geophys. J. R. Astron. Soc.*, *54*, 547–573.

Priest, E. R., G. Hornig, and D. I. Pontin (2003), On the nature of three-dimensional magnetic reconnection, *J. Geophys. Res.*, *108*(A7), 1285, doi:10.1029/2002JA009812.

Pu, Z., et al. (2005), Double Star TC-1 observations of component reconnection at the dayside magnetopause: A preliminary study, *Ann. Geophys.*, *23*(8), 2889–2895.

Pu, Z. Y., et al. (2007), Global view of dayside magnetic reconnection with the dusk-dawn IMF orientation: A statistical study for Double Star and Cluster data, *Geophys. Res. Lett.*, *34*, L20101, doi:10.1029/2007GL030336.

Schindler, K., M. Hesse, and J. Birn (1988), General magnetic reconnection, parallel electric fields, and helicity, *J. Geophys. Res.*, *93*(A6), 5547–5557.

Scurry, L., and C. T. Russell (1991), Proxy studies of energy transfer to the magnetopause, *J. Geophys. Res.*, *96*(A6), 9541–9548.

Siscoe, G. L., et al. (2001), Global role of $E_{\parallel}$ in magnetopause reconnection: An explicit demonstration, *J. Geophys. Res.*, *106*(A7), 13,015–13,022.

Sonnerup, B. U. O. (1974), Magnetopause reconnection rate, *J. Geophys. Res.*, *79*(10), 1546–1549.

Temerin, M., and X. Li (2006), Dst model for 1995–2002, *J. Geophys. Res.*, *111*, A04221, doi:10.1029/2005JA011257.

Vasyliunas, V. M. (1975), Theoretical models of magnetic field line merging, 1, *Rev. Geophys.*, *13*(1), 303–336.

Vasyliunas, V. M. (1984), Steady state aspects of magnetic field line merging, in *Magnetic Reconnection in Space and Laboratory Plasmas*, *Geophys. Monogr. Ser.*, vol. 30, edited by J. E. W. Hones, pp. 25–31, AGU, Washington, D.C.

Vasyliunas, V. M., J. R. Kan, G. L. Siscoe, and S.-I. Akasofu (1982), Scaling relations governing magnetospheric energy transfer, *Planet. Space Sci.*, *30*, 359.

Wiltberger, M., R. Weigel, M. Gehmeyr, and T. Guild (2005), Analysis and visualization of space science model output and data with CISM-DX, *J. Geophys. Res.*, *110*, A09224, doi:10.1029/2004JA010956.

J. G. Lyon, J. E. Ouellette, and B. N. Rogers, Department of Physics and Astronomy, Dartmouth College, 6127 Wilder Laboratory, Hanover, NH 03755, USA. (Jeremy.E.Ouellette.Adv09@Dartmouth.edu)

M. Wiltberger, High Altitude Observatory, National Center for Atmospheric Research, Boulder, CO 80305, USA.